

Three-dimensional time-resolved optical tomography of a conical breast phantom

Jeremy C. Hebden, Hylke Veenstra, Hamid Dehghani, Elizabeth M. C. Hillman, Martin Schweiger, Simon R. Arridge, and David T. Delpy

A 32-channel time-resolved imaging device for medical optical tomography has been employed to evaluate a scheme for imaging the human female breast. The fully automated instrument and the reconstruction procedure have been tested on a conical phantom with tissue-equivalent optical properties. The imaging protocol has been designed to obviate compression of the breast and the need for coupling fluids. Images are generated from experimental data with an iterative reconstruction algorithm that employs a three-dimensional (3D) finite-element diffusion-based forward model. Embedded regions with twice the background optical properties are revealed in separate 3D absorption and scattering images of the phantom. The implications for 3D time-resolved optical tomography of the breast are discussed. © 2001 Optical Society of America

OCIS codes: 170.3010, 170.6920, 170.6960.

1. Introduction

A principal motivation behind the increasingly intense pursuit of medical optical tomography is the potential for providing a safe and effective method of detecting and specifying breast disease. Characteristic absorption by hemoglobin and other tissue chromophores provides a means of identifying differences between normal and diseased tissues that are not necessarily evident with established diagnostic imaging methods such as x-ray mammography. As summarized elsewhere,¹ many attempts to image the breast with optical radiation over the past 70 years have made no lasting impact on diagnostic radiology. Although the absorption by breast tissues at near-infrared (NIR) wavelengths is sufficiently low to enable measurements of transmitted light to be made through thicknesses of many centimeters, scattering severely limits the spatial resolution with which internal structures can be imaged. As a consequence, imaging methods that involve direct viewing of the

breast when illuminated from behind with a simple light source have proved to have little or no diagnostic value.² Since the mid-1980s a revival of interest in so-called optical mammography has been prompted by two areas of development. The first of these is the availability of new source and detector technologies that offer potentially more useful information from measurements of light through breast tissue. Specifically, researchers have employed time- and frequency-domain systems to measure the characteristic response of breast tissues to illumination by pulsed and intensity-modulated sources, respectively. The second development is the concept of optical tomography: algorithms that enable images representing the optical properties contained within a three-dimensional (3D) volume or a two-dimensional (2D) slice to be reconstructed from a series of measurements of light transmitted between points on the surface, aided by substantial improvements in computing technology. Several research groups have recently built breast imaging systems that exploit one or both of these developments, and most have already undergone some form of preliminary clinical evaluation. Among industrial companies, Carl Zeiss³ and Siemens have both constructed prototypes based on frequency-domain instrumentation, whereas systems developed by Philips⁴ and Imaging Diagnostic Systems⁵ use a combination of optical tomography and straightforward intensity measurements. University-based groups have explored an even broader variety of approaches to

J. C. Hebden (jem@medphys.ucl.ac.uk), H. Veenstra, H. Dehghani, E. M. C. Hillman, M. Schweiger, and D. T. Delpy are with the Department of Medical Physics and Bioengineering, 11–20 Capper Street, University College London, London WC1E 6JA, UK. S. R. Arridge is with the Department of Computer Science, Gower Street, University College London, London WC1E 6BT, UK.

Received 10 August 2000; revised manuscript received 26 March 2001.

0003-6935/01/193278-10\$15.00/0

© 2001 Optical Society of America

breast imaging, including use of intensity,^{6,7} frequency-domain,^{8,9} and time-domain^{10–12} measurements.

Although some noniterative, semianalytic approaches to 3D optical tomography have been suggested, these are generally limited to cases in which the assumption of linearity is reasonable, i.e., in which the object can be represented as a small perturbation within an otherwise well-characterized background.¹³ Iterative techniques, applicable to more-arbitrary distributions of internal scattering and absorption, have been evaluated mostly for 2D imaging because of the large computational effort involved.^{14–17} A shortcut to 3D imaging has been explored, which involves reconstructing a series of transverse slices with a 2D algorithm and then combining them to generate a 3D image.¹⁸ However, since photons migrate in all three dimensions in a scattering medium, measurements made at the surface are inevitably sensitive to structure located above and below the plane of interest. The inability of 2D algorithms to account for out-of-plane structures could obviously lead to the manifestation of significant artifacts.¹⁹

At University College London we endeavor to combine a 3D optical tomography algorithm with data acquired with a 32-channel time-domain system.¹² Our reconstruction package known as TOAST (temporal optical absorption and scattering tomography) determines the optical parameters that describe an appropriate model of photon migration within an object by comparing its predictions with the measured data. The model is then adjusted iteratively to minimize the difference between the two. TOAST contains three distinct components: a finite-element-method (FEM) forward model from which to generate simulated measurements for a given distribution of internal scattering and absorbing properties; the definition of an objective function to be minimized, based on the error between model predictions and experimental data; and a scheme for adjusting the parameters of the forward model to achieve the minimization.^{20,21} In practice, TOAST accommodates data in the form of specific data types, which represent certain characteristics of the measured signal, such as temporal moments.²²

Our imaging system, described briefly in Subsection 2.A below, was designed principally as a means of imaging the cerebral oxygenation and hemodynamics of the human neonate. Compared with breast imaging, data acquisition from newborn infants is certainly more difficult, and the reconstruction requires a more sophisticated forward model in order to take into account the large variation in tissue types, including nonscattering regions. However, the demands on imaging *performance* are perhaps less severe, since brain imaging may not require particularly high spatial resolution or specificity in order to provide valuable diagnostic information.

During the past two years, the combination of TOAST and time-domain measurements has been used to image a variety of tissue-equivalent phan-

toms^{17,18} and the human forearm.²³ However, in all cases the objects were, or (in the case of the arm) assumed to be, cylindrical, and all sources and detectors were confined to a single ring. Images were generated of single transverse planes across each object, or, by means of translating the ring, 3D cylindrical volumes could be reconstructed.²⁴ The use of multiple rings of sources and detectors was recently demonstrated by Jiang *et al.*,²⁵ who employed a full 3D FEM scheme and simple intensity measurements to reconstruct images of a cylindrical phantom. However, it is evident that the application of our system to imaging of the breast must involve the use of a more appropriate and adaptable data-acquisition geometry.

For breast imaging to be clinically effective, particularly if either the presence of lesions is unknown or their location is uncertain, it is desirable that as much of the breast is imaged as possible. Some investigators achieve this by compressing the breast in a manner similar to that for x-ray mammography and then scanning one or more sources and detectors over both surfaces.^{3,6,9–11} An alternative method is to surround the breast with an array of sources and detectors and reconstruct either a cross-sectional slice^{7,8} or the entire volume.⁴ Researchers at Philips who are pursuing the latter approach have elected to fill the void between the breast and their conical array with a fluid that has optical properties closely matched to those of the breast.⁴ This benefits the reconstruction in two significant ways. First, the exterior geometry of the reconstructed volume is known exactly. And second, the coupling of the source–detector optics at the surface is constant and independent of the subject. There are also potential disadvantages. For example, it is not certain how the choice of matching fluid properties can affect the accuracy of the reconstruction. Also, there may be an insufficient restriction on patient motion during the measurement. The most significant disadvantage from our point of view is that, to make optimum use of our relatively small number of detecting channels (32), it would be necessary to construct a series of arrays to accommodate a wide range of breast sizes. Although this approach is nevertheless attractive, for our initial exploration of breast imaging we have chosen to employ a more simple method that is adaptable to breasts of all sizes and does not require a matching fluid or breast compression.

In this paper we present the results of studies on conical breast phantoms that were performed as a prelude to initial tests on human subjects. These studies were designed to test the source–detector array geometry, the imaging protocol, the data-calibration procedures, and the 3D reconstruction algorithm.

2. Experimental Methods

A. Time-Resolved Imaging System

The University of College London imaging system, known as MONSTIR (multichannel optoelectronic

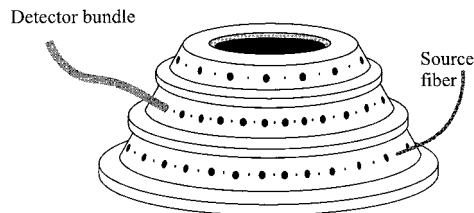


Fig. 1. Multiring fiber holder for breast imaging.

NIR system for time-resolved image reconstruction), is described in detail by Schmidt *et al.*¹² Briefly, picosecond pulses from a Ti:sapphire laser are coupled to the surface of the object via a 32-way optical fiber switch. Transmitted light is collected simultaneously by 32 detector fiber bundles. These deliver the light to four 8-anode microchannel-plate photomultiplier tubes (MCP PMTs) via 32 variable optical attenuators (VOAs), which ensure that the intensity of detected light does not saturate or damage the MCP PMTs. Each detected photon produces an electronic pulse whose arrival time is measured with respect to a laser-generated reference signal, and histograms of photon flight times (the so-called temporal point-spread functions, or TPSFs) are accumulated. The full set of TPSFs is subsequently transferred to a dedicated workstation for processing and image reconstruction.

For preliminary breast studies a conical fiber holder was constructed in the form of a series of three connecting rings, as illustrated in Fig. 1. The rings can be used in isolation, joined in pairs, or all combined, depending on the size of the breast. The design, based on an electrode array used for electrical impedance breast imaging by Holder and colleagues in London,²⁶ also facilitates the addition of further rings of larger diameter. The smallest top ring can accommodate as many as 16 source fibers and 16 detector bundles, whereas the larger rings can accommodate as many as 32 of each.

B. Conical Breast Phantoms

The optical properties of healthy and diseased breast tissues have been measured extensively by many research groups over the past 20 years, using both *in vitro*^{27–29} and *in vivo*^{30–34} methods. Most measurements of the transport scatter coefficient μ_s' of breast tissues are in the range 0.6–1.3 mm⁻¹. Values of the absorption coefficient μ_a , generally considered less reliable when measured *in vitro* because of inevitable drainage of blood,²⁹ are typically in the range 0.002–0.008 mm⁻¹. Troy *et al.*²⁹ conclude that, although their *in vitro* results exhibited no statistical difference between the average properties of healthy and diseased tissues taken over a large sample of patients, the differences for tissues taken from the same patient can be significant. Recent *in vivo* measurements reported by Tromberg *et al.*³⁴ indicated that some tumors exhibited 1.25 to threefold higher absorption than normal breast tissue. Overall, most

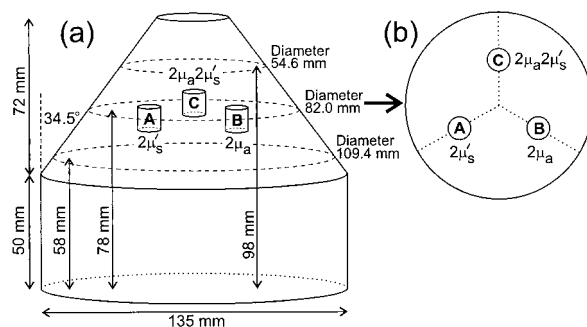


Fig. 2. (a) Breast phantom with embedded cylinders of contrasting optical properties. Dashed curves indicate the three planes of sources and detectors. (b) Middle plane indicating the cylinder locations.

evidence suggests that the ratio between the values of both μ_a and μ_s' for healthy and diseased tissues are of the order of a factor of 2.

Solid tissue-equivalent phantoms with a conical geometry suitable for use with the fiber holder described above were constructed from a mixture of titanium dioxide particles and NIR absorbing dye in epoxy resin.³⁵ A pair were made with the following uniform optical properties at a wavelength of 800 nm: $\mu_s' = 0.8 \pm 0.1 \text{ mm}^{-1}$, $\mu_a = 0.007 \pm 0.001 \text{ mm}^{-1}$, and a refractive index of 1.56. Inserted within one phantom are three cylinders with relative optical properties of (a) $2\mu_s'$ and μ_a , (b) μ_s' and $2\mu_a$, and (c) $2\mu_s'$ and $2\mu_a$. The cylinders have a height and diameter of 10 mm and are located in a single plane equidistant from the central axis, as illustrated in Fig. 2. This plane corresponds to that containing the sources and detectors of the middle ring of the fiber holder. The phantom without the embedded cylinders is designed to serve as a homogenous reference object, as described in Subsection 2.C.

C. Temporal Calibration

The conical breast phantom experiments were intended to explore two approaches to imaging. The first approach is to reconstruct images from so-called difference data recorded on phantoms with and without the embedded cylinders. TOAST thus employs differences (or ratios) calculated for specific data types. TOAST reconstructs an absolute image of the phantom of interest, assuming that the optical properties of the reference phantom are known exactly. Note that this process is not equivalent to the perturbation approach employed by some investigators,^{13,15,16} since there is no assumption of linearity and therefore no restriction on the distribution of absorption and scattering properties within the phantom of interest. The disadvantage of this approach is that it requires a reference object with closely matched geometry and well-known optical properties. The considerable advantage, however, is that the method is self-calibrating, provided that the influence of the inherent temporal response of the system on both sets of data is identical.

The second approach is to generate images from absolute data by performance of an appropriate temporal calibration of the system. The inherent temporal characteristics of 32 detecting channels of MONSTIR are not only different from one another but can vary over a period of time.¹² One can significantly reduce the temporal instability, caused mainly by thermal variation in the detection electronics, by maintaining a constant ambient temperature and performing all calibration measurements immediately before or after each imaging experiment. The fixed, channel-dependent variation arises because of differences between the lengths and dispersion properties of detector fiber bundles and electronic cables and between the pulse sampling characteristics of electronic components. Similarly, differences in the lengths of source fibers contribute toward a source-dependent offset in each TPSF measurement. Procedures for performing temporal calibration are described in detail by Hillman *et al.*¹⁹

Previous 2D experiments involving sources and detectors confined to a single circular ring have employed a so-called calibration tool consisting of a clear resin cylinder in which a small scattering target is embedded, attached to an optical fiber. The calibration procedure, described in detail elsewhere,^{12,19} involves (a) illuminating each detector via a source coupled to the target, (b) irradiating the target coupled to a detector with each source, and (c) connecting one source directly to one detector. To calibrate conical breast phantom data, another tool was constructed that is able to accommodate the conical holder. The new tool consists of a clear resin cone with the same external geometry as the phantoms shown in Fig. 2. Embedded within the tool, on the central axis, is a small scattering target in which an optical fiber is inserted. The outside surface of the tool was coated with a thin highly scattering layer directly beneath the three rings of the fiber holder. This layer diffuses the light traveling in or out of the tool and thus enables the embedded target to be coupled to every source and detector.

D. Imaging Experiments

As shown in Fig. 3, pairs of source fibers and detector bundles were distributed over the conical holder with 8 around the top ring, 8 around the middle ring, and 16 around the bottom ring. An experimental protocol was devised, which involved predefining the automated sequence in which each source fiber is illuminated and calculating the appropriate setting of each detector VOA for each source position. One can make an initial estimate of the settings by calculating the source-detector distances and assuming an exponential decrease in intensity with distance. For the conical breast phantom experiments the distances between sources and detectors vary from a few millimeters to a maximum of 110 mm. To record adequate signal for the largest separations, it is desirable to maximize the source power, which was approximately 50 mW. Although the maximum finite attenuation achieved by the detector VOAs is ~ 3 op-



Fig. 3. Breast phantom imaging experiment.

tical densities (ODs), large source intensities will produce photon count rates at many detectors closer to a given source, which go beyond the capacity of the VOA to produce an acceptable minimum (approximately 3×10^5 photons/s). For example, it was estimated that, for a source in the top ring, recording adequate signal in all detectors in the bottom ring would require most detectors in the top ring to be deactivated (i.e., VOAs set to zero transmission). Consequently, data were acquired from each source position *twice*, with two different source intensities. MONSTIR includes a computer-controlled source attenuator, which can provide up to ~ 2.5 ODs of attenuation of the light entering the 32-way fiber switch. The protocol employed for these experiments therefore involved illuminating sources for 30 s at a high (~ 50 -mW) power and then illuminating for a further 30 s following a 2-OD attenuation. For a given source position, detectors at near and intermediate distances were deactivated during the first sequence and then activated during the second. Although it was not a necessary condition, no detectors were activated for both sequences. However, some detectors close to a source were deactivated for both sequences, and therefore only 29 or 30 TPSFs were recorded for each source.

Immediately prior to acquiring data on phantoms, a series of calibration measurements were performed with the tool described in Subsection 2.C. An additional calibration measurement was introduced as a means of compensating for low-level ($< 0.5\%$) cross talk between adjacent MCP PMT channels. This involved measuring the cross-talk intensity as each detector is illuminated in sequence, by use of the calibration tool. These data are then used to apply a minor correction to TPSFs recorded on a given channel by subtraction of a small fraction of signal measured on adjacent channels. Appropriate temporal calibration corrections were then performed upon the data acquired on the phantoms with and without the embedded cylinders in order to produce a series of

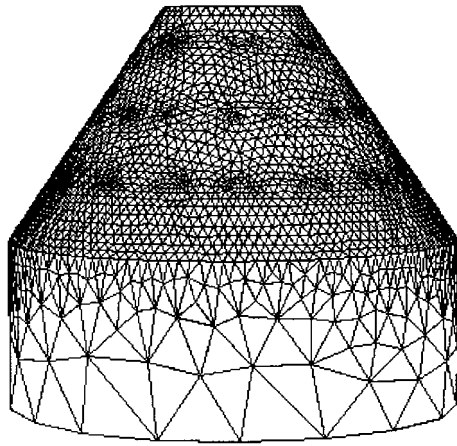


Fig. 4. 3D FEM mesh for cone imaging experiments.

data types suitable for image reconstruction with TOAST. The calibrated data types generated for the production of images of absolute optical properties were mean time and variance.

Although simulations have shown that measurements of intensity are useful for optical tomography in combination with other data types,²² the strong sensitivity of intensity to photon interactions at the surface renders it difficult to calibrate. Thus it becomes necessary to either employ differences in log intensity measured in response to some change in internal optical properties³⁶ or incorporate a variable surface coupling coefficient into the reconstruction process.³⁷ For the experiments described here, involving two phantoms with similar, uniform surfaces, an assumption is made that the coupling for a given source or detector remains unchanged as the fiber holder is transferred from one phantom to the other. In other words, use of intensity is restricted to so-called difference imaging, with the difference in log intensity measured for phantoms with and without the embedded cylinders. Likewise, neither mean time nor variance requires precalibration for difference imaging.²³ It is necessary to calculate mean time and variance only directly from the raw uncalibrated TPSFs and assume that the temporal response of the system (including delays, broadening, and the like) is identical for corresponding source-detector pairs.

3. Image Reconstruction

A. Three-Dimensional Finite-Element-Method Model

To reconstruct 3D images with TOAST, a 3D finite-element mesh was generated with a Delaunay triangulation algorithm³⁸ and is illustrated in Fig. 4. The mesh has an external geometry identical to that of the conical breast phantoms and consists of 36,857 second-order tetrahedral elements that have a total of 57,766 nodes. Special care was taken to ensure that the mesh density was high enough near regions of rapidly changing field (near source and detector

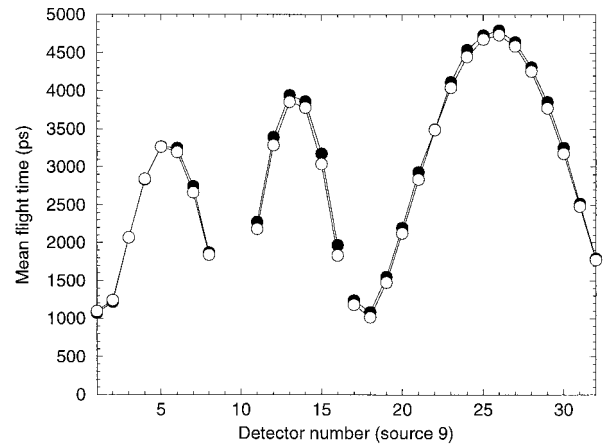


Fig. 5. Mean flight values for each detector and for source 9 obtained from experimental data (filled circles) and forward-model predictions (open circles).

positions) to facilitate an accurate forward calculation.

As a preliminary check on the validity of the forward model and on the quality of the data, data types predicted by the model were compared with experimental values. With the known positions of the sources and detectors, and fixed optical properties for both the homogenous and cylinder-containing phantoms, two sets of simulated data were generated for mean time and for intensity. It was found that the most favorable match between the model and experimental values of mean time for the homogenous phantom corresponds to a transport scatter coefficient of $\mu_{s'} = 1.0 \text{ mm}^{-1}$ and an absorption coefficient of $\mu_a = 0.007 \text{ mm}^{-1}$. The model and experimental values of mean time for source 9 (located in the middle ring) are plotted in Fig. 5. Note that detectors 9 and 10 were located adjacent to source 9 on either side and were therefore deactivated. The discrepancy between the nominal transport scattering coefficient of the solid phantoms and that of the best-match FEM model is assumed to be due to a larger-than-expected experimental error during the manufacture of the phantoms.

The simulated values of mean time and the logarithm of intensity from the homogenous model were then subtracted from the values predicted by the model of the phantom with the cylinders. The differences for the model data types for source 9 and the corresponding differences calculated from the experimental data are shown in Figs. 6 and 7. The trends observed in the data correspond well with those predicted by the model in both cases, and similar correspondence was observed in results obtained for all other sources. Some discrepancy between model and data is inevitable, owing to small (<5-mm) uncertainties in the positioning of the embedded cylinders within the phantoms, and in the relative positioning of the holder. A further error in the log intensity difference values will be due to variability

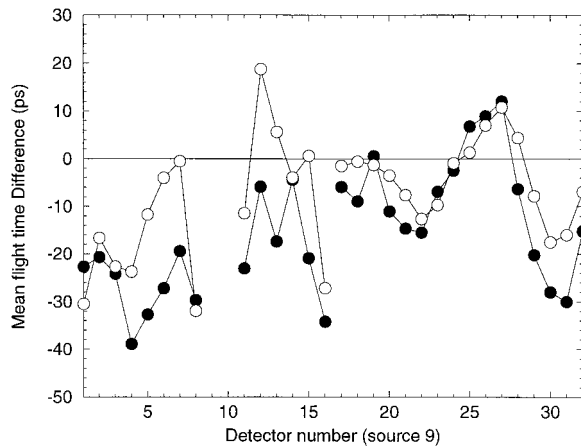


Fig. 6. Differences between the values of mean flight time generated for phantoms with and without the embedded cylinders: experimental data (filled circles) and forward-model predictions (open circles).

in the surface coupling coefficient for each source and detector between the two phantom measurements. As indicated above, although this is a relatively minor problem for phantoms with identical featureless surfaces, this is potentially a significant difficulty for routine imaging of human tissues.

The small differences in mean flight time exhibited by both the model and the data (less than 20 ps for nearly all source–detector combinations) had unfortunate implications for our attempts to generate absolute images from calibrated data. To reveal the internal cylinders, the error in the calibration must not exceed the magnitude of the difference signal. Unfortunately the actual uncertainty in absolute mean time determined from multiple measurements made with the new calibration tool is ~ 20 ps. The uncertainty stems from an inherent source- and detector-dependent variability in the contribution of the new calibration tool to the overall temporal re-

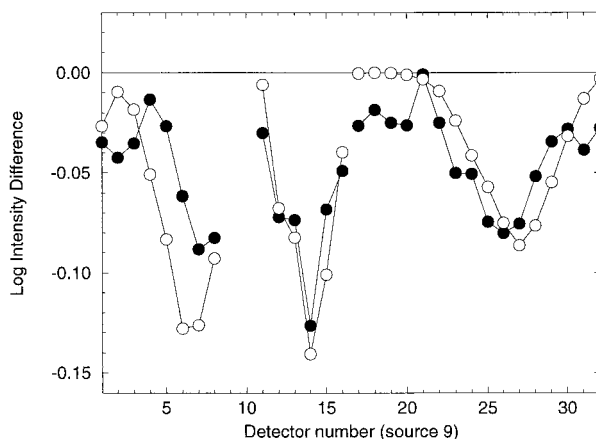


Fig. 7. Differences between the values of log intensity generated for phantoms with and without the embedded cylinders: experimental data (filled circles) and forward-model predictions (open circles).

sponse. The calibration uncertainty was found to be even more significant for variance. As a consequence, only difference imaging was possible.

B. Difference Images

The difference data generated for intensity and mean time were employed to reconstruct the entire volume of the phantom as represented by the FEM mesh described above. Differences in variance generally exhibited more noise than the other two data types and therefore were not used in the reconstruction. The 3D reconstruction algorithm, as described by Arridge *et al.*,²⁴ employed an initial estimate in the form of a cone with uniform optical properties of $\mu_s' = 1.0 \text{ mm}^{-1}$ and $\mu_a = 0.007 \text{ mm}^{-1}$. Images of the internal distribution of absorption and scatter differences were reconstructed simultaneously from log intensity and mean-time differences, with a nonlinear conjugate-gradient method. The sources were modeled as an isotropic Gaussian source (width of 2 mm), placed one scattering distance (1 mm) inside the outer boundary, and a Robin boundary condition was used.³⁹ The image was reconstructed into a $32 \times 32 \times 18$ pixel basis with median filtering at each iteration.

Image reconstruction was performed on a 450-MHz Pentium personal computer with 1 Gbyte of RAM and required several hours per iteration. The results achieved after six iterations are shown in Figs. 8 and 9. These show the reconstructed absorption and scattering properties, respectively, for a series of ten transverse slices, each averaged over a 6-mm thickness. The image at the height of 78 mm represents the transverse slice containing the centers of the embedded cylinders. Bright regions corresponding to all three embedded cylinders are evident, located at the expected lateral and vertical positions. Cylinder C, representing a perturbation in both scatter and absorption, is the most dominant feature in both sets of images. The other two cylinders, representing perturbations in just one parameter, are revealed most clearly in the image corresponding to that parameter. However, they are apparent to a lesser degree in the other image, too. The observed contrast of cylinders for both absorption and scattering images in each case is roughly 10% of background intensity instead of the expected 100%. This may be at least partly due to the finite spatial resolution. The observed features are roughly twice the diameter of the actual cylinders, which corresponds to a factor of 8 increase in volume. Imprecise knowledge of the exact optical properties of the reference phantom may also influence the quantitative accuracy.

4. Discussion

Experimentation on suitable tissue-equivalent phantoms is necessary to evaluate both the instrumentation and the reconstruction software prior to trials on human subjects and to establish that it is possible to produce images with data acquired by use of safe exposures over a realistic period of time. In these

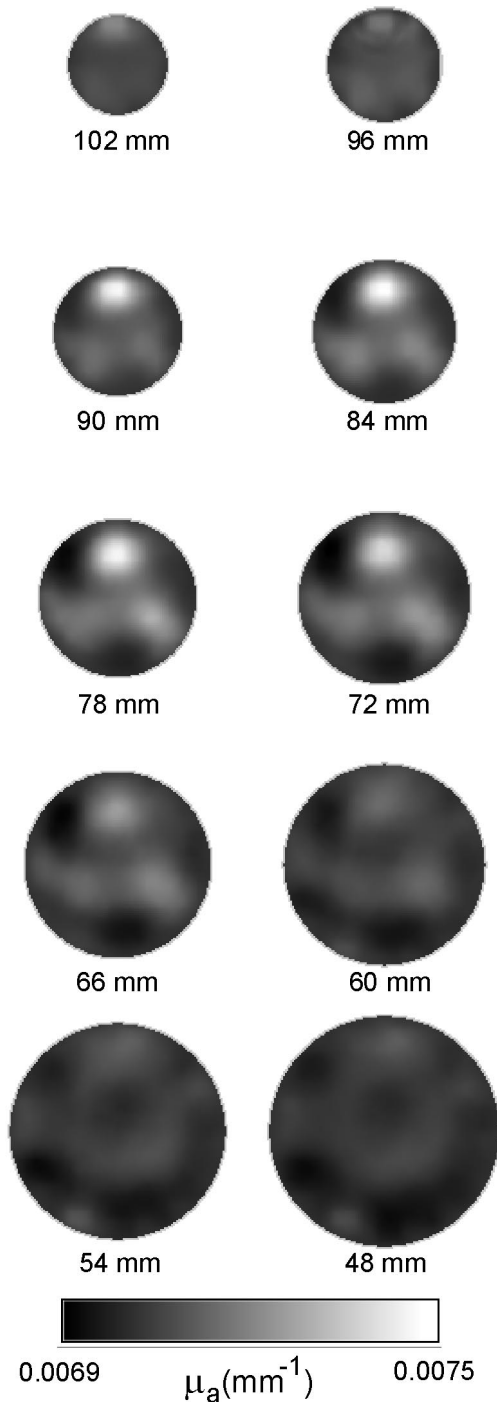


Fig. 8. Absorption properties of the cone reconstructed in 3D from differences in intensity and mean time, displayed as a series of transverse slices. Heights above the base of the phantom are indicated.

respects the experiments described above provide a positive prognosis for clinical imaging with the chosen protocol. The results also represent the first 3D optical images of a tissue-equivalent object acquired with time-resolved data without involving physical translation of sources or detectors.

The cylinders embedded in the conical breast phantom produced subtle perturbations to the time-

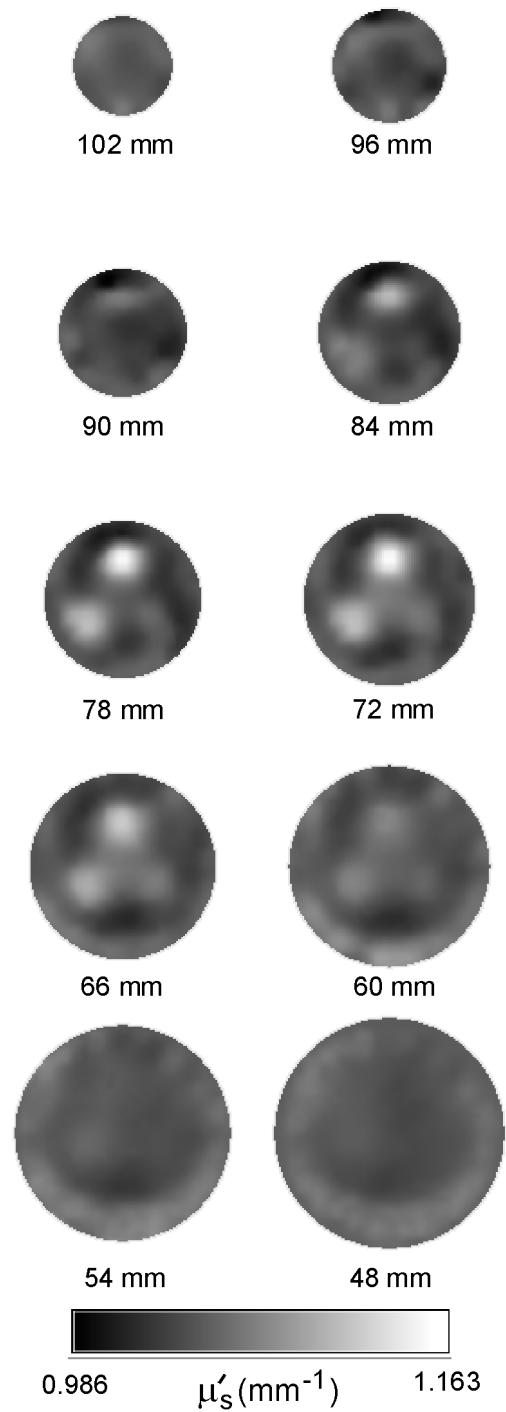


Fig. 9. Scattering properties of the cone reconstructed in 3D from differences in intensity and mean time, displayed as a series of transverse slices. Heights above the base of the phantom are indicated.

resolved signals compared with those measured on the corresponding homogenous phantom. The combination of measurements made on both phantoms enabled these perturbations to be successfully isolated, resulting in the reconstruction of difference-images that reveal all three cylinders with good localization and contrast. Good separation between scatter and absorption is observed, and images con-

tain remarkably few artifacts. For optical mammography to become clinically useful, it is probable that quantitative information must be derived to distinguish diseased lesions from healthy breast tissues, particularly since spatial resolution is limited and distinction based purely on morphology is unlikely. However, accurate recovery of local absorption and scattering coefficients may be limited by the finite spatial resolution. Almost certainly a clinical manifestation of optical mammography must exploit the variability of absorption of certain tissues with wavelength. In particular, differences between the inherent absorption by oxyhemoglobin and deoxyhemoglobin provide the facility to map tissue oxygenation. A two-wavelength NIR probe that measures backscattered light from the breast was recently employed by Zhu *et al.*⁴⁰ to study the blood concentration and oxygenation of prediagnosed lesions. Their results indicate that optical imaging may significantly improve the ability to distinguish between benign from malignant tissue compared with ultrasound imaging alone.

In a separate series of experiments, 2D images of the same phantoms were acquired with the 32 sources and 32 detectors confined to a single ring around the plane in which the embedded cylinders were centered. Difference data generated for intensity and mean time were used in a 2D reconstruction algorithm to produce cross-section images, published elsewhere.⁴¹ The embedded cylinders were revealed with resolution and contrast comparable with that exhibited in Figs. 8 and 9 for the same plane (78 mm above the base). Both theory and experiment have shown that absolute imaging using 2D algorithms can give rise to significant artifacts, owing to the inevitable mismatch between real (3D) data and the predictions of a 2D FEM model.^{19,41} However, this mismatch largely cancels for difference imaging of objects such as the cone phantoms presented here, which contain no out-of-plane structure. For breast imaging, however, features may occur in any plane, and 2D difference imaging is likely to fail.

A portable dual-wavelength pulsed laser is currently being incorporated into the MONSTIR imaging system. It is feasible that the use of dual-wavelength data may also provide a convenient solution to the problem of calibration. Instead of employing a homogenous phantom as a reference, perhaps difference imaging could be performed with data acquired at one wavelength as a reference for data acquired at another. This approach facilitates a full calibration of the system temporal response and the intensity coupling coefficients but may not be effective if the optical properties of the breast at the reference wavelength are highly nonuniform or different in magnitude from the properties at the other wavelength. The likely effectiveness of this method is currently being investigated with both experiments and simulations.⁴¹ Alternatively, differences can be calculated between data obtained before and after the administration of appropriate contrast agents, as recently demonstrated by Ntziachristos *et al.*³⁶ An-

other approach to breast imaging that has been proposed is to perform difference imaging on data collected on the left and right breasts of the same subject. The accuracy of this method will inevitably depend on the degree of homogeneity in the breast used as the reference and therefore may have limited applicability.

Prior to the start of studies on suitable patients and volunteers, a new design of fiber holder is currently being evaluated. The surface area illuminated by each source has been increased to facilitate a decrease in irradiance without requiring a significant reduction in total power. This has been achieved by withdrawal of the ends of the source fibers by 10 mm and allowing the inherent divergence of the emitted beam to illuminate a circular area of 6-mm diameter. Increasing the source illumination area also reduces the dependency of intensity measurements on small-scale irregularities in the surface coupling. The new holder will have a geometry similar to that of the holder employed for phantom experiments, although in the future we envisage producing a larger collection of interconnecting rings of different diameters and cone angles to accommodate a much greater variety of breast shapes and sizes. Meanwhile, new calibration procedures are being explored that enable the temporal characteristics of the imaging system to be evaluated more accurately, without requiring a calibration tool.

Each phantom measurement involved a total exposure time of 2×32 sources \times 30 s, plus \sim 3-s system dead time between each source. This corresponds to a total acquisition time of \sim 35 min. This is certainly too long for routine clinical use, and the effect of reducing acquisition time on image quality needs to be explored. Ultimately the total exposure time will depend on the attenuating properties of the tissue and the tolerance of the chosen data types to stochastic noise. However, the need to scan at two source intensities could be eliminated in the future by means of increasing the dynamic range of the detector VOAs. Also unacceptably long for clinical use was the period required for reconstructing the images. However, a preliminary test with a 3D mesh with a lower density (36,636 nodes) and a forward mesh reconstruction basis suggested that images of comparable quality can be achieved at speeds of only 47 min per iteration. The availability of faster computers will obviously lead to further decreases in reconstruction time.

Finally, we invite other researchers in the biomedical optics community to borrow our phantoms to evaluate their own reconstruction techniques and instrumentation. More details about the availability of phantoms, as well as information regarding the exchange of data and reconstruction software, are available on our website: www.medphys.ucl.ac.uk/research/borg.

Support for this research has been generously provided by the Wellcome Trust and the Engineering and Physical Sciences Research Council.

References

1. J. C. Hebden and D. T. Delpy, "Diagnostic imaging with light," *Brit. J. Radiol.* **70**, 206–214 (1997).
2. B. Monsees, J. M. Destouet, and W. G. Totty, "Light scanning versus mammography in breast cancer detection," *Radiology* **163**, 463–465 (1987).
3. M. Kaschke, H. Jess, G. Gaida, J. Kaltenbach, and W. Wrobel, "Transillumination imaging of tissue by phase modulation techniques," in *Advances in Optical Imaging and Photon Migration*, R. R. Alfano, ed., Vol. 24 of OSA Proceedings Series (Optical Society of America, Washington, D.C., 1994), pp. 88–92.
4. S. B. Colak, D. G. Papaioannou, G. W. 't Hooft, M. B. van der Mark, H. Schomberg, J. C. J. Paasschens, J. B. M. Melissen, and N. van Asten, "Tomographic image reconstruction from optical projections in light-diffusing media," *Appl. Opt.* **36**, 180–213 (1997).
5. R. J. Grable, D. P. Rohler, and K. L. A. Sastry, "Optical tomography breast imaging," in *Optical Tomography and Spectroscopy of Tissue: Theory, Instrumentation, Model, and Human Studies II*, B. Chance and R. R. Alfano, eds., Proc. SPIE **2979**, 197–210 (1997).
6. P. He, M. Kaneko, M. Takai, K. Baba, Y. Yamashita, and K. Ohta, "Breast cancer diagnosis by laser transmission photo-scanning with spectro-analysis," *Radiation Med.* **8**, 1–5 (1990).
7. S. Nioka, Y. Yung, M. Shnall, S. Zhao, S. Orel, C. Xie, B. Chance, and L. Solin, "Optical imaging of breast tumor by means of continuous waves," *Adv. Exp. Med. Biol.* **411**, 227–232 (1997).
8. B. W. Pogue, M. Testorf, T. McBride, U. Osterberg, and K. Paulsen, "Instrumentation and design of a frequency-domain diffuse optical tomography imager for breast cancer detection," *Opt. Express* **1**, 391–403 (1997), <http://www.opticsexpress.org>.
9. M.-A. Franceschini, K. T. Moesta, S. Fantini, G. Gaida, E. Gratton, H. Jess, W. W. Mantulin, M. Seeber, P. M. Schlag, and M. Kaschke, "Frequency-domain techniques enhance optical mammography: initial clinical results," *Proc. Natl. Acad. Sci. USA* **94**, 6468–6473 (1997).
10. V. Ntziachristos, X. Ma, and B. Chance, "Time-correlated single photon counting imager for simultaneous magnetic resonance and near-infrared mammography," *Rev. Sci. Instrum.* **69**, 4221–4233 (1998).
11. D. Grosenick, H. Wabnitz, H. H. Rinneberg, T. Moesta, and P. M. Schlag, "Development of a time-domain optical mammograph and first *in vivo* applications," *Appl. Opt.* **38**, 2927–2943 (1999).
12. F. E. W. Schmidt, M. E. Fry, E. M. C. Hillman, J. C. Hebden, and D. T. Delpy, "A 32-channel time-resolved instrument for medical optical tomography," *Rev. Sci. Instrum.* **71**, 256–265 (2000).
13. W. Cai, B. B. Das, F. Liu, F. A. Zeng, M. Lax, and R. R. Alfano, "Three dimensional image reconstruction in highly scattering turbid media," in *Optical Tomography and Spectroscopy of Tissue: Theory, Instrumentation, Model, and Human Studies II*, B. Chance and R. R. Alfano, eds., Proc. SPIE **2979**, 241–244 (1997).
14. H. Jiang, K. D. Paulsen, U. L. Osterberg, and M. S. Patterson, "Improved continuous light diffusion imaging in single- and multi-target tissue-like phantoms," *Phys. Med. Biol.* **43**, 675–693 (1998).
15. U. Hampel and R. Freyer, "Fast reconstruction for optical absorption tomography in media with radially symmetric boundaries," *Med. Phys.* **25**, 92–101 (1998).
16. R. Model, M. Orlt, M. Walzel, and R. Hünlich, "Optical imaging: three-dimensional approximation and perturbation approaches for time-domain data," *Appl. Opt.* **37**, 7968–7976 (1998).
17. J. C. Hebden, F. E. W. Schmidt, M. E. Fry, M. Schweiger, E. M. C. Hillman, and D. T. Delpy, "Simultaneous reconstruction of absorption and scattering images by multichannel measurement of purely temporal data," *Opt. Lett.* **24**, 534–536 (1999).
18. F. E. W. Schmidt, J. C. Hebden, E. M. C. Hillman, M. E. Fry, M. Schweiger, D. T. Delpy, and S. R. Arridge, "Multiple-slice imaging of a tissue-equivalent phantom by use of time-resolved optical tomography," *Appl. Opt.* **39**, 3380–3387 (2000).
19. E. M. C. Hillman, J. C. Hebden, F. E. W. Schmidt, S. R. Arridge, M. Schweiger, H. Dehghani, and D. T. Delpy, "Calibration techniques and datatype extraction for time-resolved optical tomography," *Rev. Sci. Instrum.* **71**, 3415–3427 (2000).
20. M. Schweiger and S. R. Arridge, "A system for solving the forward and inverse problems in optical spectroscopy and imaging," in *Advances in Optical Imaging and Photon Migration*, Vol. 2 of 1996 OSA Trends in Optics and Photonics Series (Optical Society of America, Washington, D.C., 1996), pp. 263–268.
21. S. R. Arridge, "Optical tomography in medical imaging," *Inverse Problems* **15**, R41–R93 (1999).
22. M. Schweiger and S. R. Arridge, "Application of temporal filters to time resolved data in optical tomography," *Phys. Med. Biol.* **44**, 1699–1717 (1999).
23. E. M. C. Hillman, J. C. Hebden, M. Schweiger, H. Dehghani, F. E. W. Schmidt, D. T. Delpy, and S. R. Arridge, "Time resolved optical tomography of the human forearm," *Phys. Med. Biol.* **46**, 1117–1130 (2001).
24. S. R. Arridge, J. C. Hebden, M. Schweiger, F. E. W. Schmidt, M. E. Fry, E. M. C. Hillman, H. Dehghani, and D. T. Delpy, "A method for 3D time-resolved optical tomography," *Int. J. Imaging Syst. Technol.* **11**, 2–11 (2000).
25. H. Jiang, Y. Xu, and N. Iftimia, "Experimental three-dimensional optical image reconstruction of heterogeneous turbid media from continuous-wave data," *Opt. Express* **7**, 204–209 (2000), <http://www.opticsexpress.org>.
26. D. S. Holder, "Design and electrical characteristics of an electrode array for electrical impedance tomography of the female breast," *Innov. Tech. Biol. Med.* **16**, 144–150 (1995).
27. V. G. Peters, D. R. Wyman, M. S. Patterson, and G. L. Frank, "Optical properties of normal and diseased human breast tissues in the visible and near infrared," *Phys. Med. Biol.* **35**, 1317–1334 (1990).
28. H. Key, E. R. Davies, P. C. Jackson, and P. N. T. Wells, "Optical characteristics of breast tissues at visible and near-infrared wavelengths," *Phys. Med. Biol.* **36**, 579–590 (1991).
29. T. L. Troy, D. L. Page, and E. M. Sevick-Muraca, "Optical properties of normal and diseased breast tissues: prognosis for optical mammography," *J. Biomed. Opt.* **1**, 342–355 (1996).
30. K. Suzuki, Y. Yamashita, K. Ohta, M. Kaneko, M. Yoshida, and B. Chance, "Quantitative measurement of optical parameters in normal breasts using time-resolved spectroscopy: *in vivo* results of 30 Japanese women," *J. Biomed. Opt.* **1**, 330–334 (1996).
31. H. Heusmann, J. Kölzer, and G. Mitic, "Characterization of female breasts *in vivo* by time resolved and spectroscopic measurements in near infrared spectroscopy," *J. Biomed. Opt.* **1**, 425–434 (1996).
32. M. J. Holboke, B. J. Tromberg, X. Li, N. Shah, J. Fishkin, D. Kidney, J. Butler, B. Chance, and A. G. Yodh, "Three-dimensional diffuse optical mammography with ultrasound localization in a human subject," *J. Biomed. Opt.* **5**, 237–247 (2000).
33. V. Quaresima, S. J. Matcher, and M. Ferrari, "Identification and quantification of intrinsic optical contrast for near-infrared mammography," *Photochem. Photobiol.* **67**, 4–14 (1998).

34. B. J. Tromberg, N. Shah, R. Lanning, A. Cerussi, J. Espinoza, T. Pham, L. Svaasand, and J. Butler, "Non-invasive *in vivo* characterization of breast tumors using photon migration spectroscopy," *Neoplasia* **2**, 26–40 (2000).
35. M. Firbank, M. Oda, and D. T. Delpy, "An improved design for a stable and reproducible phantom material for use in near-infrared spectroscopy and imaging," *Phys. Med. Biol.* **40**, 955–961 (1995).
36. V. Ntziachristos, B. Chance, and A. G. Yodh, "Differential diffuse optical tomography," *Opt. Express* **5**, 230–242 (1999), <http://www.opticsexpress.org>.
37. D. A. Boas, T. Gaudette, and S. R. Arridge, "Simultaneous imaging and optode calibration with diffuse optical tomography," *Opt. Express* **8**, 263–270 (2001), <http://www.opticsexpress.org>.
38. J. Schoeberl, "NETGEN—an automatic 3D tetrahedral mesh generator," <http://www.sfb013.uni-linz.ac.at/~joachim/netgen/> (2000).
39. M. Schweiger, S. R. Arridge, M. Hiraoka, and D. T. Delpy, "The finite element method for the propagation of light in scattering media: boundary and source conditions," *Med. Phys.* **22**, 1779–1792 (1995).
40. Q. Zhu, E. Conant, and B. Chance, "Optical imaging as an adjunct to sonograph in differentiating benign from malignant breast lesions," *J. Biomed. Opt.* **5**, 229–236 (2000).
41. E. M. C. Hillman, H. Dehghani, J. C. Hebden, S. R. Arridge, M. Schweiger, F. M. Gonzalez-Barbosa, and D. T. Delpy, "Development of 3D *in-vivo* time-resolved optical tomography using simulations of complex structures," in *Optical Tomography and Spectroscopy of Tissue IV*, B. Chance, R. R. Alfano, B. J. Tromberg, M. Tamura, and E. M. Sevick-Muraca, eds., *Proc. SPIE* **4250** (to be published).